We are IntechOpen, the world's leading publisher of Open Access books Built by scientists, for scientists

4,800
Open access books available

122,000
International authors and editors

135M
Downloads

Our authors are among the

154
Countries delivered to

TOP 1%
most cited scientists

12.2%
Contributors from top 500 universities

CLARIVATE ANALYTICS BOOK CITATION INDEX INDEXED

WEB OF SCIENCE™

Selection of our books indexed in the Book Citation Index in Web of Science™ Core Collection (BKCI)

Interested in publishing with us?
Contact book.department@intechopen.com

Numbers displayed above are based on latest data collected.
For more information visit www.intechopen.com

6

CI/OFDM Underwater Acoustic Communication System

Fang Xu and Ru Xu
Xiamen University
China

1. Introduction

The underwater acoustic channel (UAC) is one of the most challenging environments to be encountered for the communication. Because of the absorption of the signal, the path loss depends on the signal frequency (Berkhovskikh & Lysanov, 2003; Jensen et al., 2011). Multipath transmission causes intersymbol interference (ISI), and it extends over tens to hundreds of milliseconds according to the communication distance (Stojanovic & Preisig, 2009). Since the velocity of sound in water is about 1500m/s, any relative motion includes the transmitter or receiver and even surface waves will cause non-negligible Doppler effects, including shifting and spreading. All these phenomena dramatically limit the data rate achievable and the performance of the communications. The bandwidth is very limited, and the system is actually a broadband communication system because the center frequency of the signal is always at the same order of the bandwidth (Stojanovic, 1996; Stojanovic, 2007; Stojanovic & Preisig, 2009).

In order to achieve high data rate, it is important to use bandwidth-efficient modulation methods in UAC. Multi-carrier modulation is one of the candidates that can be used. Orthogonal Frequency Division Multiplexing (OFDM) (Lam & Ormondroyd, 1997; Kim & Lu, 2000; Stojanovic, 2006; Stojanovic, 2008; Li et al., 2008), direct-sequence spread-spectrum (DSSS) (Freitag et al. 2001; Frassati et al. 2005), frequency-hopped spread-spectrum (FHSS) (Stojanovic, 1998; Freitag et al., 2001) and code-division multiple access (CDMA) (Charalampos et al. 2001; Stojanovic & Freitag, 2006; Tsimenidis, 2001)were used in UAC channels in recent years and much literature focus on the conceptual system analysis and computer simulations.

In this chapter, we introduce a new multi-carrier modulation into the UAC channels which is called Carrier Interferometry OFDM (CI/OFDM) (Nassar et al., 1999; Wiegandt & Nassar, 2001; Nassar et al., 2002a, 2002b). Compared with OFDM, the CI/OFDM has a low PAPR characteristic and inherent frequency selective combining, which makes it a very attractive signaling scheme in frequency selective fading channels (Wiegandt & Nassar, 2001; Wiegandt et al., 2001; Wiegandt & Nassar, 2003; Wiegandt et al., 2004).

The chapter is organized as follows. In Section II, the characteristics of CI signal are analyzed. Two algorithms are proposed in Section III. Details are focused on the PAPR performance, and new algorithms to complete the modulation and demodulation of the

CI/OFDM. The configuration of the CI/OFDM underwater acoustic communication system is presented in Section IV. Furthermore, the key algorithms including synchronization, channel estimation and equalization are described. In Section V, Performance results for different field tests are summarized. Conclusions are drawn in Section VI.

2. CI/OFDM signals

2.1 The theory of the CI/OFDM

In CI/OFDM transmitter, after serial to parallel transform, information symbols are modulated onto all the N parallel subcarriers and then added linearly together to get the output signal (Nassar et al. 2002). As shown in Fig.1 , the output of the signal is

$$s(t)=\sum_{k=0}^{N-1}s_k(t)=\mathrm{Re}\left\{\sum_{k=0}^{N-1}a_k c_k(t)\right\}\quad 0\le t\le T \tag{1}$$

where $s_k(t)$ is the modulated signal for the kth information symbol a_k . $\mathrm{Re}(\cdot)$ is the real part of the signal and $c_k(t)$ is the kth CI signal, which can be express by

$$c_k(t)=\sum_{i=0}^{N-1}e^{j2\pi i\Delta ft}\cdot e^{j\theta_k^i} \tag{2}$$

It is easy to see that $c_k(t)$ is a multi-carrier signal with different phase offsets $\theta_k^i=(2\pi/N)\cdot k\cdot i$. Submit (2) into (1), we get the continuous baseband transmitted signal

$$s(t)=\mathrm{Re}\left\{\sum_{k=0}^{N-1}a_k\sum_{i=0}^{N-1}e^{j2\pi i\Delta ft}\cdot e^{j\frac{2\pi}{N}ki}\right\}\quad 0\le t\le T \tag{3}$$

We rewrite the discrete form of (3) with the Nyquist sampling rate of $f_s=N\Delta f$

$$s(n)=\mathrm{Re}\left\{\sum_{k=0}^{N-1}a_k\sum_{i=0}^{N-1}e^{j\frac{2\pi}{N}in}\cdot e^{j\frac{2\pi}{N}ik}\right\}\quad n=0,1,...,N-1 \tag{4}$$

where $\Delta f=1/T_s$ (T_s is one CI/OFDM symbol duration) to ensure orthogonality among subcarriers, and $(2\pi/N)k\cdot i$ is the phase offset used for a_k which ensures the orthogonality among the N information symbols.

After transmitted over a frequency selective fading channel, the received signal at receiver side is

$$r(n)=\sum_{k=0}^{N-1}\sum_{i=0}^{N-1}\alpha_i a_k e^{j\frac{2\pi}{N}in}\cdot e^{j\frac{2\pi}{N}ik}\cdot e^{j\phi_i}+w(n)\quad n=0,1,...,N-1 \tag{5}$$

where α_i and ϕ_i are the amplitude fade and phase offset on the ith carrier, respectively. $w(n)$ is the addictive white Gaussian noise (AWGN).

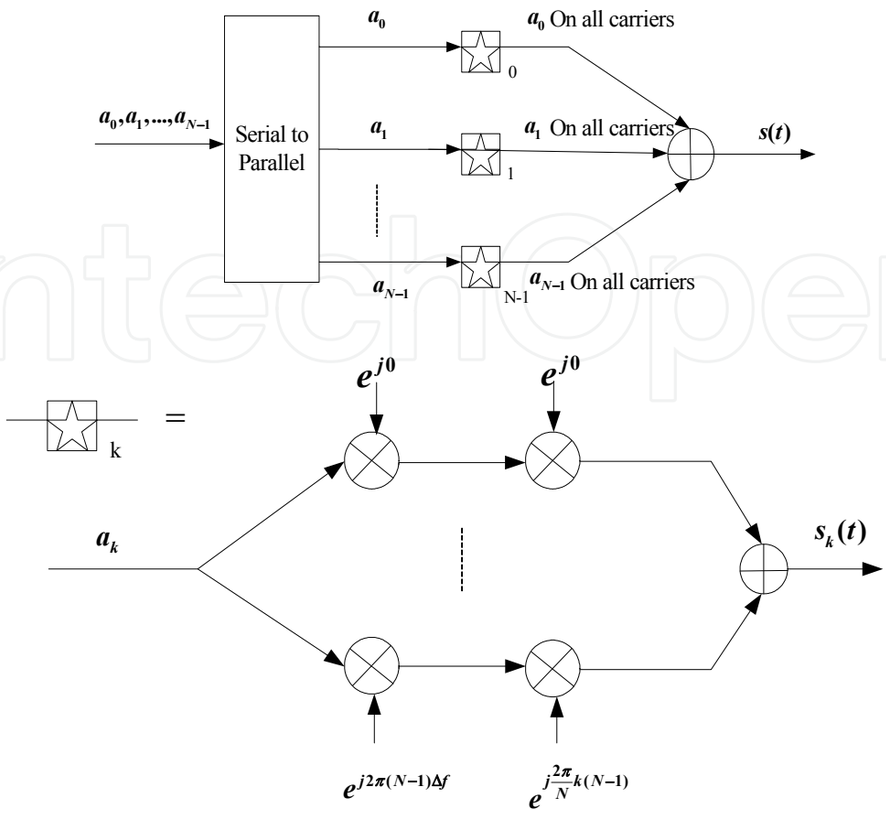

Fig. 1. The conceptual CI/OFDM Transmitter

Fig.2 depicts the modulation theory of CI/OFDM in transmitter and the detection of the kth symbol signal at the receiver side (Nassar et al. 2002). Assume perfect synchronization, the received signal is first projected onto the N orthogonal carriers, multi-carrier demodulation and phase offsets remove are carried out after that. This leads to the decision vector $r^k = (r_0^k, r_1^k, ..., r_{N-1}^k)$ for the information symbol a_k, where r_i^k is defined as

$$r_i^k = A\alpha_i a_k + A \cdot \sum_{j=0, j\neq k}^{N-1} \alpha_i a_j \cos(\theta_k^i - \theta_j^i) + w_i \tag{6}$$

The first part of (6) is the desired information symbol which is randomly faded by factor α_i, and the second part is the interferences of the other N-1 information symbols which modulated on the same carrier.

Different combining strategies are employed to help restore orthogonality between subcarriers. In AWGN channel, the optimal combining is equal gain combining (EGC). After performing $C = \sum_{i=0}^{N-1} r_i$, interferences are close to zero. While in frequency selective channel, different combining strategies are used to get combining gains, for example, the maximum ratio combining (MRC), the minimum mean square error combining (MMSEC) (Itagkai & Adachi, 2004). After combining, the signals are sent to the detector.

As presented to date, the implementation of original CI/OFDM is complicated, and it is important to note that the receiver is designed for detecting only one information symbol. Although CI/OFDM had been proved that it could improve BER performance by exploiting frequency diversity and depress the PAPR simultaneously, its implementation was complicated and only conceptual transmitter and receiver models had been given in the literature.

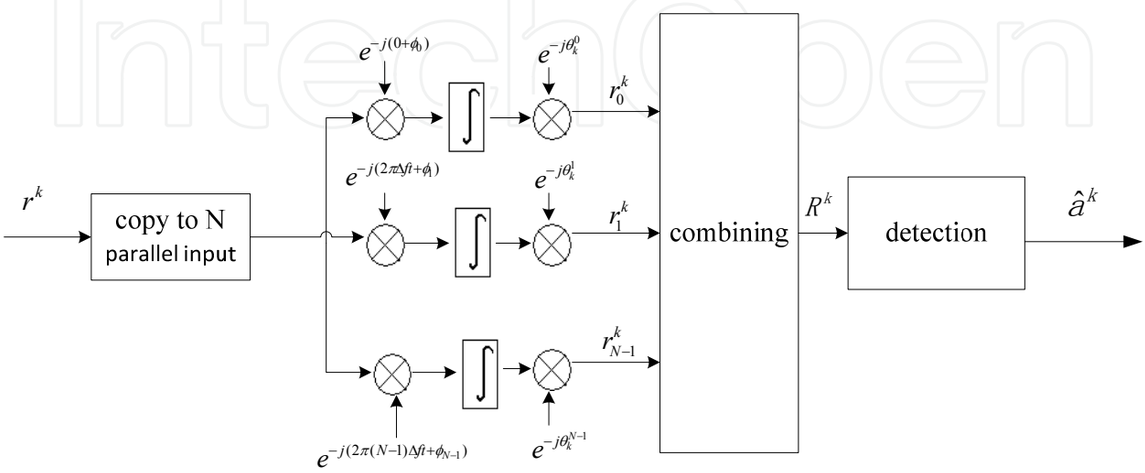

Fig. 2. The CI/OFDM receiver for the kth symbol

2.2 The characteristics of the CI signal

The baseband CI signal (Nassar et al. 2002) is given bellow

$$c(t) = \sum_{i=0}^{N-1} e^{j2\pi i\Delta ft} \tag{7}$$

where N is the number of the subcarriers and Δf is the interval of the subcarriers. It is obviously that CI signal is a periodic signal. Simulation results are shown in Fig. 3. In simulations, $N = 8$, $\Delta f = 1Hz$, the width of the main lobe and the side lobe are $2/(N\Delta f) = 0.125s$ and $1/(N\Delta f) = 0.0625s$, respectively. By selecting optimal phase offsets, CI signals are orthogonal to each other.

We rewrite the discrete CI signal as bellow

$$c(n) = \sum_{i=0}^{N-1} e^{j\frac{2\pi}{N}in} \tag{8}$$

It is clearly that the discrete CI signal is the result of sampling a rectangle pulse with the sampling rate Δf in the frequency domain. It has constant amplitude (CA).

Based on the analysis of the CI signal, two novel algorithms for CI/OFDM modulation and demodulation are presented in this chapter.

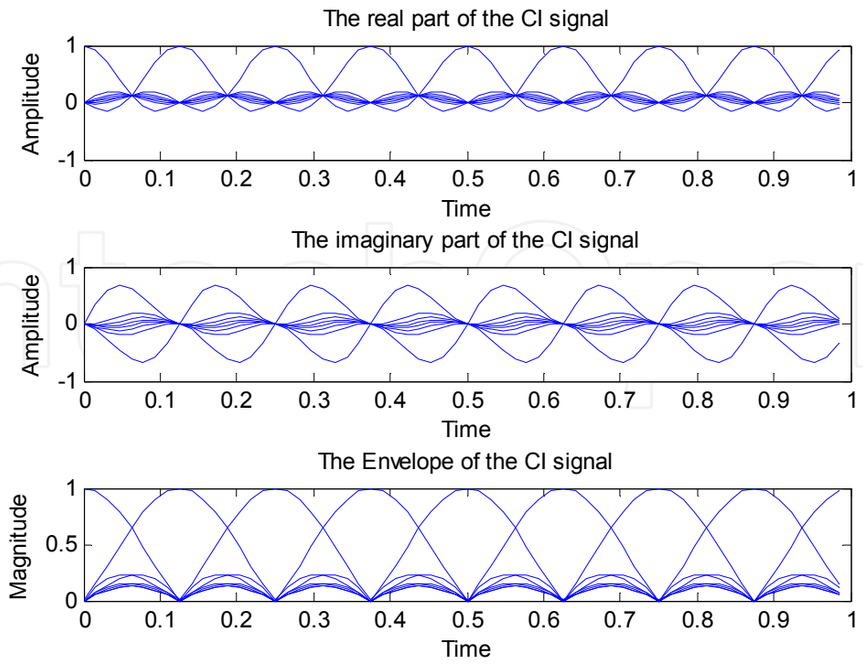

Fig. 3. Baseband CI signals

3. Proposed algorithms

3.1 Multi-carrier algorithm

As in (4), the discrete kth transmitted symbol is

$$s(n) = \sum_{i=0}^{N-1} (a_k \cdot e^{j\frac{2\pi}{N}ik}) e^{j\frac{2\pi}{N}in} \quad n = 0,1,...,N-1 \tag{9}$$

It is obviously that (9) is an inverse discrete Fourier transform (IDFT) with weighting efficients $a_k \cdot e^{j\frac{2\pi}{N}ik}$ which change with the index k and i. The IDFT weighting coefficient can be written as a matrix

$$\begin{bmatrix} a_0 \cdot e^{j\frac{2\pi}{N}i\cdot 0} \\ a_1 \cdot e^{j\frac{2\pi}{N}i\cdot 1} \\ \vdots \\ a_k \cdot e^{j\frac{2\pi}{N}i\cdot k} \\ \vdots \\ a_{N-1} \cdot e^{j\frac{2\pi}{N}i\cdot (N-1)} \end{bmatrix} = \begin{bmatrix} a_0 e^{j\frac{2\pi}{N}\cdot 0\cdot 0} & a_0 e^{j\frac{2\pi}{N}\cdot 1\cdot 0} & \cdots & a_0 e^{j\frac{2\pi}{N}\cdot i\cdot 0} & \cdots & a_0 e^{j\frac{2\pi}{N}\cdot (N-1)\cdot 0} \\ a_1 e^{j\frac{2\pi}{N}\cdot 0\cdot 1} & a_1 e^{j\frac{2\pi}{N}\cdot 1\cdot 1} & \cdots & a_1 e^{j\frac{2\pi}{N}\cdot i\cdot 1} & \cdots & a_1 e^{j\frac{2\pi}{N}\cdot (N-1)\cdot 1} \\ \vdots & \vdots & \vdots & \vdots & \vdots & \vdots \\ a_k e^{j\frac{2\pi}{N}\cdot 0\cdot k} & a_k e^{j\frac{2\pi}{N}\cdot 1\cdot k} & \vdots & a_k e^{j\frac{2\pi}{N}\cdot i\cdot k} & \vdots & a_k e^{j\frac{2\pi}{N}\cdot (N-1)\cdot k} \\ \vdots & \vdots & \cdots & \vdots & \cdots & \vdots \\ \underbrace{a_{N-1} e^{j\frac{2\pi}{N}\cdot 0\cdot (N-1)}}_{0^{\#}\text{subcarrier}} & \underbrace{a_{N-1} e^{j\frac{2\pi}{N}\cdot 1\cdot (N-1)}}_{1^{\#}\text{subcarrier}} & \cdots & \underbrace{a_{N-1} e^{j\frac{2\pi}{N}\cdot i\cdot (N-1)}}_{i^{\#}\text{subcarrier}} & \cdots & \underbrace{a_{N-1} e^{j\frac{2\pi}{N}\cdot (N-1)\cdot (N-1)}}_{(N-1)^{\#}\text{subcarrier}} \end{bmatrix} \tag{10}$$

Since i is the index of subcarrier, the columns of the matrix are corresponding to different subcarriers, that is

$$\left[\underbrace{\sum_{k=0}^{N-1} a_k e^{j\frac{2\pi}{N}\cdot 0\cdot k}}_{0^{\#}\text{subcarrier}} \quad \underbrace{\sum_{k=0}^{N-1} a_k e^{j\frac{2\pi}{N}\cdot 1\cdot k}}_{1^{\#}\text{subcarrier}} \quad \cdots \quad \underbrace{\sum_{k=0}^{N-1} a_k e^{j\frac{2\pi}{N}\cdot i\cdot k}}_{i^{\#}\text{subcarrier}} \quad \cdots \quad \underbrace{\sum_{k=0}^{N-1} a_k e^{j\frac{2\pi}{N}\cdot (N-1)\cdot k}}_{(N-1)^{\#}\text{subcarrier}}\right] \tag{11}$$

(11) implies that the coefficient of the IDFT can also be corresponding to another IDFT (Xu et al., 2007a, 2007b). Hence, the CI/OFDM modulation model employed in this chapter corresponds to

$$\begin{aligned} s(n) &= \sum_{k=0}^{N-1} a_k c_k\left(\frac{nTs}{N}\right) \\ &= \sum_{k=0}^{N-1} a_k \sum_{i=0}^{N-1} e^{j\frac{2\pi}{N}ki} e^{j\frac{2\pi}{N}ni} \\ &= \sum_{i=0}^{N-1} \left(\sum_{k=0}^{N-1} a_k e^{j\frac{2\pi}{N}ki}\right) e^{j\frac{2\pi}{N}ni} \\ &= N \cdot \underset{n}{IDFT}\left[N \cdot \underset{i}{IDFT}(a_k)\right] \\ &= N^2 \cdot \underset{n}{IDFT}\left[\underset{i}{IDFT}(a_k)\right] \qquad n = 0,1,...,N-1 \end{aligned} \tag{12}$$

Fig.4 shows a block diagram of the proposed system. At the transmitter side, the input data is first mapped into a baseband constellation. Then the data sequence is converted to parallel and enters the first IDFT to perform CI spreading. After that, the second IDFT is

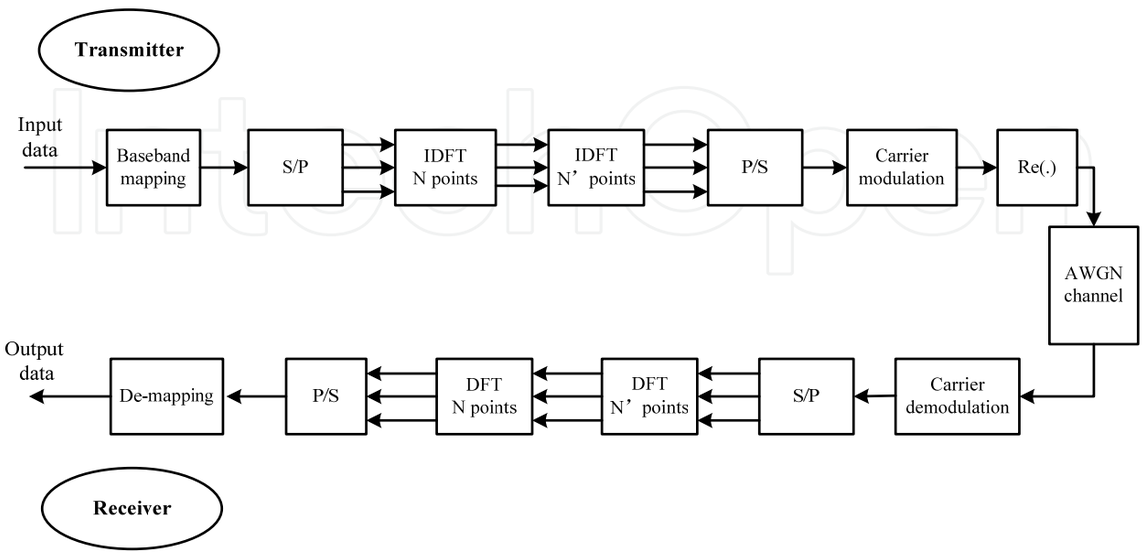

Fig. 4. The block diagram of the multi-carrier algorithm

used to implement orthogonal multi-carrier modulation. Parallel data is first transformed to serial data, then the complex base-band signal is then up-converted to the transmission frequency, and the real part of the signal is sent out to the channel. In the receiver, the signal is first down-converted to the base-band. Serial to parallel transformation followed by orthogonal multi-carrier demodulated which completed by the first discrete Fourier transform (DFT). Then CI code de-spreading is implemented by the second DFT and finally, the phase constellation of the data is extracted (Xu et al. 2007).

3.2 Single-carrier algorithm

The CI spread code in (10) is similar to the polyphase codes (Heimiller, 1961). Polyphase codes were proven to have good periodic correlation properties, the sequence is

$$1,1,...,1,1,\xi_1,\xi_2,\xi_3,....,\xi_{p-1},1,\xi_1^2,\xi_2^2,...,\xi_{p-1}^2,1,\xi_1^3,\xi_2^3,...,\xi_{p-1}^3,1,\xi_1^{p-1},\xi_2^{p-1},...,\xi_{p-1}^{p-1} \tag{13}$$

where $\xi_k = e^{-j(2\pi k/p)}$, $0 \le k \le p-1$ is a primitive Pth root of unity, the sequence has zero periodic correlation except for the peaks at $i = 0, p^2, 2p^2, \ldots$.

Polyphase code were proven to be a constant amplitude , zero autocorrelation (CAZAC) sequence (Heimiller, 1961). According to the characteristics of the CAZAC sequence, if u_i is a CAZAC sequence, then $\overline{u}_i$, where $\overline{u}$ denotes complex conjugation, is also a CAZAC sequence (Milewski, 1983). Note that the orthogonality, periodicity, constant amplitude and zero autocorrelation are not changed, it suggests a new way of thinking about constructing new CI signals.

In this chapter, the new CI signals are complex conjugations of primary CI signals (Nassar et al. 2002), which can be written as

$$\begin{bmatrix} a_0 \cdot e^{-j\frac{2\pi}{N}i\cdot 0} \\ a_1 \cdot e^{-j\frac{2\pi}{N}i\cdot 1} \\ \vdots \\ a_k \cdot e^{-j\frac{2\pi}{N}i\cdot k} \\ \vdots \\ a_{N-1} \cdot e^{-j\frac{2\pi}{N}i\cdot (N-1)} \end{bmatrix} = \begin{bmatrix} a_0 e^{-j\frac{2\pi}{N}\cdot 0\cdot 0} & a_0 e^{-j\frac{2\pi}{N}\cdot 1\cdot 0} & \cdots & a_0 e^{-j\frac{2\pi}{N}\cdot i\cdot 0} & \cdots & a_0 e^{-j\frac{2\pi}{N}\cdot (N-1)\cdot 0} \\ a_1 e^{-j\frac{2\pi}{N}\cdot 0\cdot 1} & a_1 e^{-j\frac{2\pi}{N}\cdot 1\cdot 1} & \cdots & a_1 e^{-j\frac{2\pi}{N}\cdot i\cdot 1} & \cdots & a_1 e^{-j\frac{2\pi}{N}\cdot (N-1)\cdot 1} \\ \vdots & \vdots & \vdots & \vdots & \vdots & \vdots \\ a_k e^{-j\frac{2\pi}{N}\cdot 0\cdot k} & a_k e^{-j\frac{2\pi}{N}\cdot 1\cdot k} & \vdots & a_k e^{-j\frac{2\pi}{N}\cdot i\cdot k} & \vdots & a_k e^{-j\frac{2\pi}{N}\cdot (N-1)\cdot k} \\ \vdots & \vdots & \cdots & \vdots & \cdots & \vdots \\ \underbrace{a_{N-1} e^{-j\frac{2\pi}{N}\cdot 0\cdot (N-1)}}_{0^{\#}\text{subcarrier}} & \underbrace{a_{N-1} e^{-j\frac{2\pi}{N}\cdot 1\cdot (N-1)}}_{1^{\#}\text{subcarrier}} & \cdots & \underbrace{a_{N-1} e^{-j\frac{2\pi}{N}\cdot i\cdot (N-1)}}_{i^{\#}\text{subcarrier}} & \cdots & \underbrace{a_{N-1} e^{-j\frac{2\pi}{N}\cdot (N-1)\cdot (N-1)}}_{(N-1)^{\#}\text{subcarrier}} \end{bmatrix} \tag{14}$$

Then, the CI/OFDM signal is mathematically characterized by the following equation

Fig.5 shows the proposed system using the single-carrier algorithm. In the transmitter, the input data is mapping into a baseband constellation. Then the data sequence is converted to parallel and enters the first DFT to perform CI spreading. After that, the IDFT is used to implement orthogonal multi-carrier modulation. The complex baseband signal is then up-converted to the transmission frequency.

$$
\begin{aligned}
s(n) &= \sum_{k=0}^{N-1} a_k c_k \left(\frac{nTs}{N}\right) = \sum_{k=0}^{N-1}\sum_{i=0}^{N-1} a_k e^{-j\frac{2\pi}{N}ki} e^{j\frac{2\pi}{N}ni} \\
&= \sum_{i=0}^{N-1}\left(\sum_{k=0}^{N-1} a_k e^{-j\frac{2\pi}{N}ki}\right) e^{j\frac{2\pi}{N}ni} \\
&= N \cdot \underset{n}{IDFT}\left[\underset{i}{DFT}(a_k)\right] \qquad n = 0,1,...,N-1
\end{aligned}
\tag{15}
$$

In the receiver, the signal is down-converted to the baseband. After serial to parallel transformation, the signal is first demodulated by DFT, Then CI de-spreading is implemented by the IDFT and the phase constellation of the data is extracted.

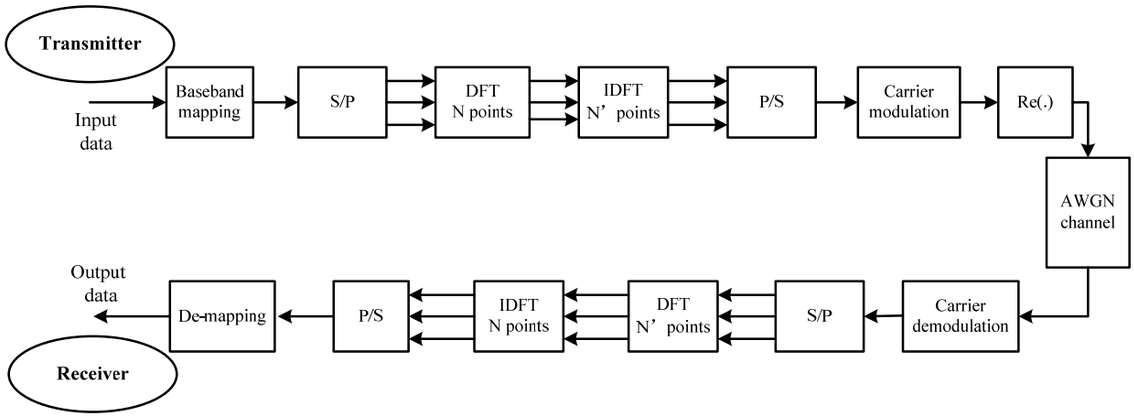

Fig. 5. The block diagram of the single-carrier algorithm

3.3 The comparisons between the conceptual CI/OFDM and the proposed algorithms

In the conceptual model of CI/OFDM, the computational complexity increases with the number of parallel information symbols dramatically, which make it unpractical to the engineering. In the conceptual model of CI/OFDM, the CI spreading needs $N \times N$ complex multiplications $N \times (N-1)$ complex additions. While in multi-carrier algorithm or single-carrier algorithm, only $N/2\log_2 N$ complex multiplications and $N\log_2 N$ complex additions are needed. For example, when $N = 1024$, we need 1048576 complex multiplications and 1046529 complex additions in conceptual CI/OFDM, while only 5120 complex multiplications and 10240 complex additions are needed in our algorithms.

Of course, the two algorithms have their own problems. As in the multi-carrier method, the physical concept is not very clear, since there are two cascaded IDFT in the transmitter which may cause confusion about the transformation between the frequency domain and time domain. On the other hand, in the single-carrier method, filter should be well designed to compress the bandwidth of the output signal.

As shown in fig.6, the performance of CI/OFDM system is verified under AWGN channel. We replace the IDFT by the inverse fast Fourier transform (IFFT) due to the efficiency of the algorithm. It is obviously that there is no difference between the conceptual CI/OFDM and the two algorithms proposed in this chapter.

Since lower PAPR is the most important characteristic of CI/OFDM, and the algorithms presented here are somewhat different from the theoretical realization of the CI/OFDM, it is reasonable for us to verify the PAPR performance based on these two algorithms. Fig. 7 shows the simulation result. A conclusion can be drawn that the two algorithms presented in this chapter have the same PAPR and BER performance as the conceptual CI/OFDM, and lower complexity which make it applicable to engineering.

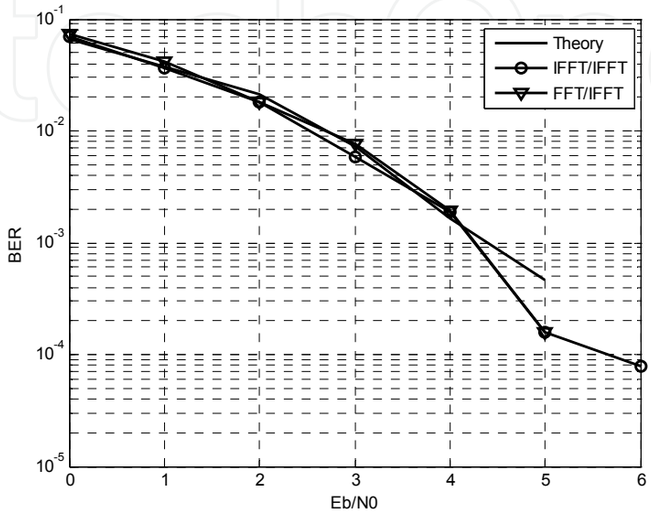

Fig. 6. Performance comparisons of three algorithms under AWGN channels

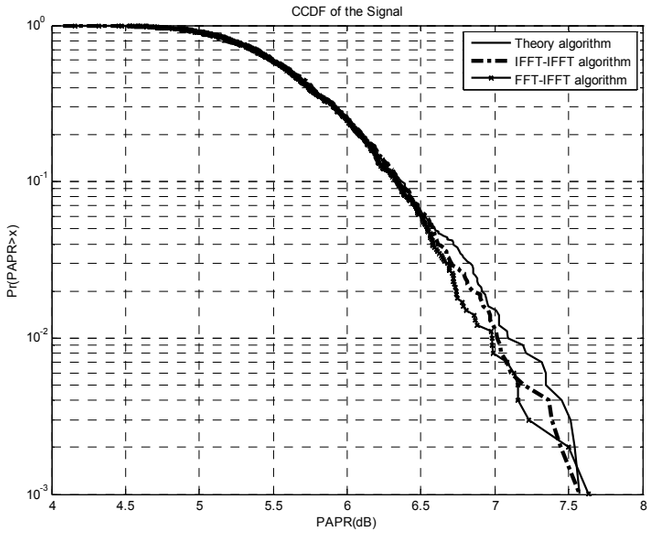

Fig. 7. PAPR Performance comparisons of three algorithms

4. Configuration of the CI/OFDM underwater acoustic communication system

Based on the aforementioned algorithms, two CI/OFDM underwater acoustic communication systems are proposed. Simplified block diagrams of the proposed systems are shown in Fig.8 and Fig.9. We also replace the IDFT by the IFFT due to the efficiency of the algorithm.

As shown in Fig.8, based on the multi-carrier algorithm, the input data is first coded by Low Density Parity Check Codes (LDPC). After baseband mapping, the data sequence is converted to parallel and enters the first IFFT to perform CI spreading. Pilot signals are inserted before the second IFFT. The second IFFT is used to implement orthogonal multi-carrier modulation. A cyclic prefix and postfix are also appended to the data sequence as guard intervals in order to combat the ISI induced by the multi-path delay spread in the UWA channel. The complex base-band signal is then up-converted to the transmission frequency and the real part of the signal is sent out to the UWA channel by the transducer.

In the receiver, the signal is first down-converted to the base-band. Then the signal is demodulated by the first FFT. Channel estimation is performed to track the channel response and compensations of the signal are performed. Then CI code de-spreading is implemented by the second FFT, and finally, the phase constellation of the data is extracted.

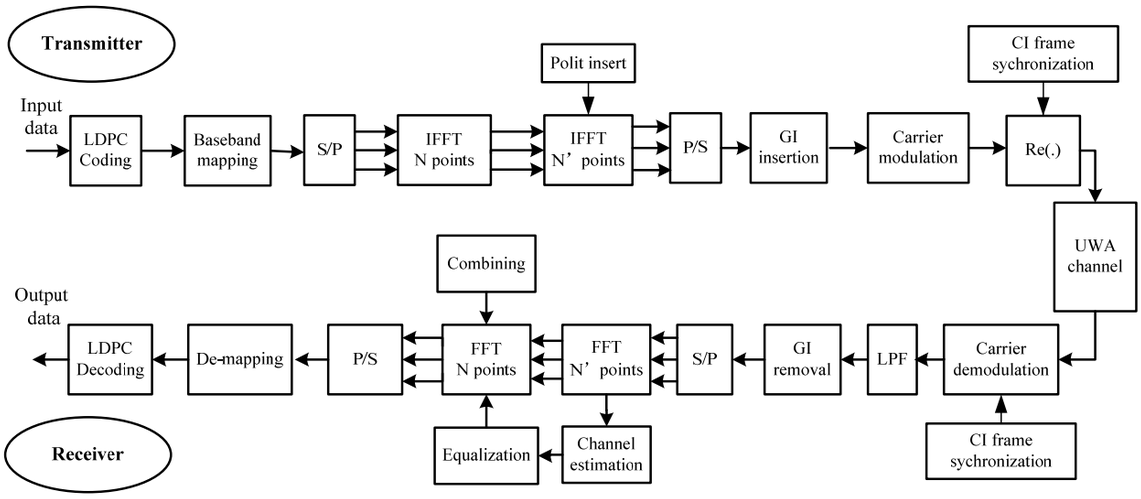

Fig. 8. The block diagram of the system based on multi-carrier algorithm

Fig.9 shows a simplified block diagram of the proposed system based on single-carrier algorithm. In the transmitter, the input data is first encoded by LDPC and then mapping into a baseband constellation. The data sequence is converted to parallel and enters the first FFT to perform CI spreading. After that, the IFFT is used to implement orthogonal multi-carrier modulation. A cyclic prefix is also appended as a guard interval to the data sequence in order to combat the inter ISI induced by multipath delay spread in the selective fading channel. In addition, a pilot signal is appended for the purposes of channel estimation in the receiver. The complex baseband signal is then up-converted to the transmission frequency. In the receiver, the signal is down-converted to baseband. The signal is first demodulated by FFT, and diversity combining scheme is employed as frequency-domain equalization where the combining weights are estimated by the pilot signal. Then de-spreading is implemented by the IFFT and the phase constellation of the data is extracted. Finally, the data is mapped back to the binary form, and a soft LDPC decoding is performed.

We here focus on the multi-carrier algorithm and explain the key technologies used in the underwater acoustic communication system.

4.1 Synchronization

We use Linear Frequency Modulation (LFM) (Rihaczek, 1969; Shaw & Srivastava, 2007) signal to get coarse synchronization and CI complex spreading sequence to get accurate synchronization and fractional frequency offset estimation.

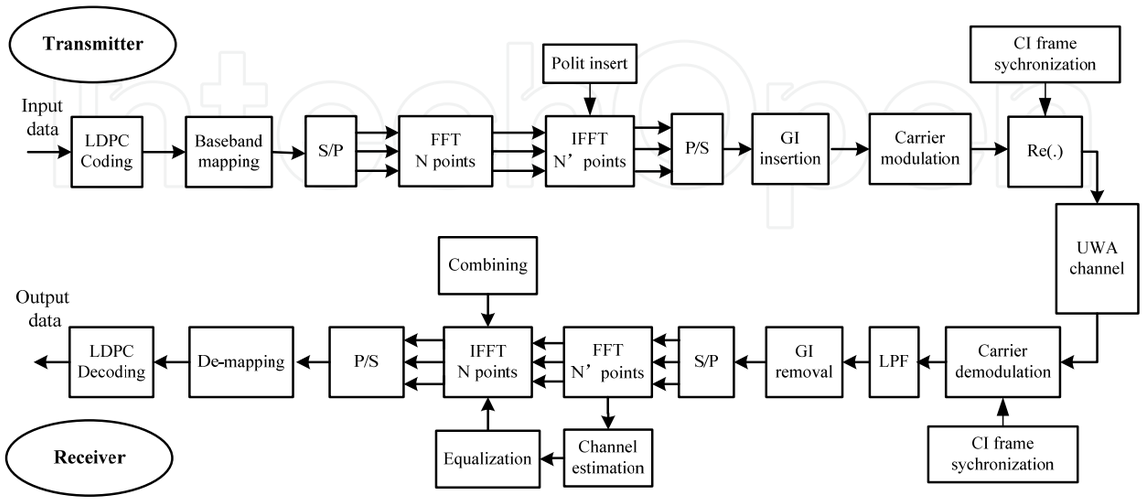

Fig. 9. The block diagram of the system based on single-carrier algorithm

4.1.1 Coarse synchronization

The expression for LFM signal is given as

$$s(t) = A \cdot rect(\frac{t}{T}) e^{j2\pi\left(f_0 t + \frac{1}{2}ut^2\right)} \tag{16}$$

where A is the amplitude of the signal, T is the width of the signal, f_0 is the carrier frequency, u is the gradient of the instantaneous frequency which is called chirp rate, $u = 2\pi B/T$. $rect(\cdot)$ is a rectangle function, defined as

$$rect(\frac{t}{T}) = \begin{cases} 1, & \left|\frac{t}{T}\right| \le \frac{1}{2} \\ 0, & \left|\frac{t}{T}\right| > \frac{1}{2} \end{cases} \tag{17}$$

Since the ambiguity function of LFM signals is wide in Doppler axis (Rihaczek, 1969), it is highly tolerant of the Doppler shift which makes it useful in mobile wireless communication systems.

4.1.2 Fine synchronization and fractional frequency shift estimation

Two identical CI complex sequences are used as fine synchronization signals and sliding correlator is applied at the receiver side to obtain the correlation peak. CI complex sequences is given by

$$1,1,...,1,1,\xi_1,\xi_2,\xi_3,....,\xi_{N-1},1,\xi_1^2,\xi_2^2,...,\xi_{N-1}^2,1,\xi_1^3,\xi_2^3,...,\xi_{N-1}^3,1,\xi_1^{N-1},\xi_2^{N-1},...,\xi_{N-1}^{N-1} \quad (18)$$

where $\xi_k = e^{j(2\pi k/N)}$, $0 \le k \le N-1$. Suppose the two received sequences are $r_1(m)$ and $r_2(m)$ (Hlaing et al. 2003; Ren, 2005), the cross-correlation function of the two sequences is

$$R(n) = \sum_{m=0}^{L-1} (r_1^*(m) r_2(m+n)) \quad (19)$$

where the L is the length of the sequence. Since the sequences are identical at the transmitter, the impact of the channel is assumed to be same to the two sequences, (18) can be written as

$$R(n) = \sum_{m=0}^{L-1} \left(r_1^*(m) r_2(m+n) \right) = \sum_{m=0}^{L-1} \left(r_1^*(m) r_1(m+L+n) \right) \quad (20)$$

The cross-correlation of two sequences can be changed into auto-correlation of one sequence, that is

$$R(0) = \sum_{m=0}^{L-1} \left(r_1^*(m) r_2(m) \right) = \sum_{m=0}^{L-1} \left(r_1^*(m) r_1(m+L) \right) \quad (21)$$

The time offset can be estimated from

$$\hat{n} = \arg\max_n \left(|R(n)|^2 \right) \quad (22)$$

Assuming that the frame synchronization is accurate, the difference between two CI complex sequences can be approximately regarded as the result of the frequency shift

$$\theta = angle(R(\hat{n})) \quad (23)$$

$$\Delta f = \theta / (2\pi T/2) = \theta / (\pi T) \quad (24)$$

where Δf is the fractional frequency shift, θ is the phase offset caused by frequency shift, T is the period of the synchronization signal which is equals to the CI/OFDM signal.

Fig. 10 shows the sliding correlation peaks of LFM signal and CI complex sequence at the receiver side in AWGN channel.

4.2 Channel estimation and equalization

When the pilot is a CAZAC sequence, it was proven that in the presence of noise, the mean square error of the channel response estimation is minus (Milewski, 1983). The mean square error equals to the variance of the noise in the channel, that is

$$E(\sum_i |\hat{r}_i - r_i|^2) = L\sigma^2 \sum_i |v_i|^2 = \sigma^2 \quad (25)$$

where $v_i \in V$, $V = 1/U$, U is the Fourier transform of the pilot sequence.

Two kinds of pilot sequences which are both CAZAC sequences are chosen to estimate the underwater acoustic channel response.

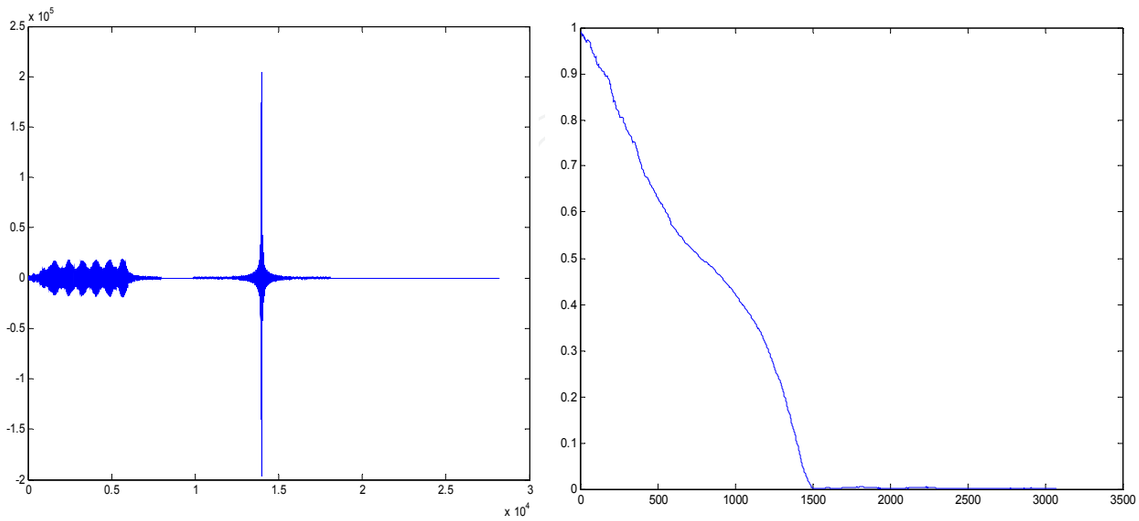

Fig. 10. Sliding correlation peak under AWGN channel. (a) Peak of LFM signal (b) Peak of CI spreading sequence

4.2.1 Pilot

1. CI complex sequence

CI complex sequence was given in equation (18). It is easy to prove the CAZAC feature of the CI complex sequence. Fig. 11 gives simulation results of the CI complex sequence.

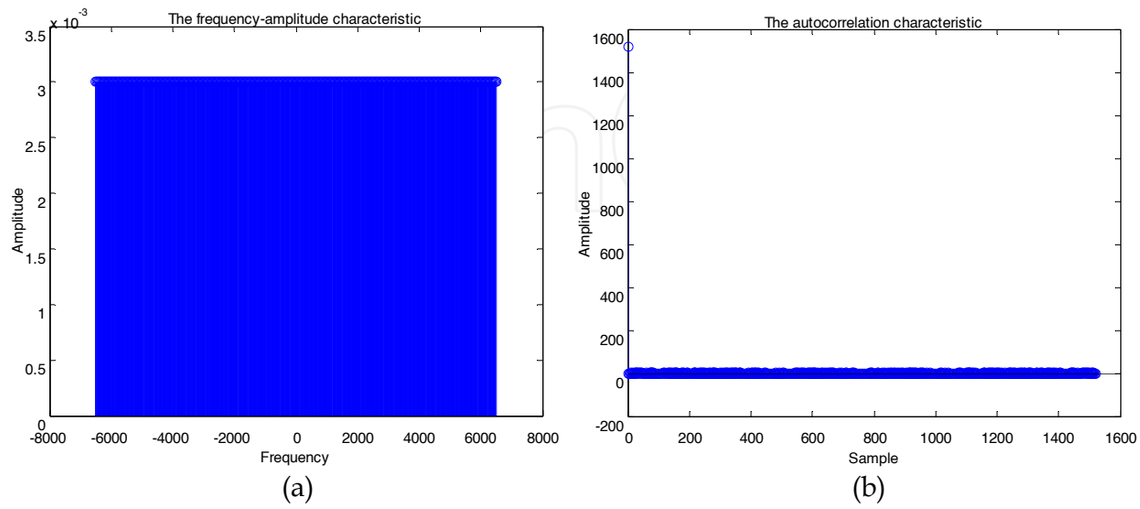

Fig. 11. The CAZAC feature of the CI complex sequence. (a) constant amplitude (b) zero autocorrelation

2. CHU sequence

CHU sequence is a polyphase code with a periodic autocorrelation function (CHU, 1972). It was proven that the CHU sequence can be constructed for any code length. When N is even, CHU sequence is defined as $a_k = \exp(i\frac{M\pi k^2}{N})$. When N is odd, it is $a_k = \exp(i\frac{M\pi k(k+1)}{N})$, where M is an integer relatively prime to N. Fig. 12 shows the amplitude-frequency and autocorrelation results of CHU sequence. Fig. 13 and Fig.14 show the channel impulse respond estimated by CI complex sequence and CHU sequence under AWGN and 4-path Rayleigh channel.

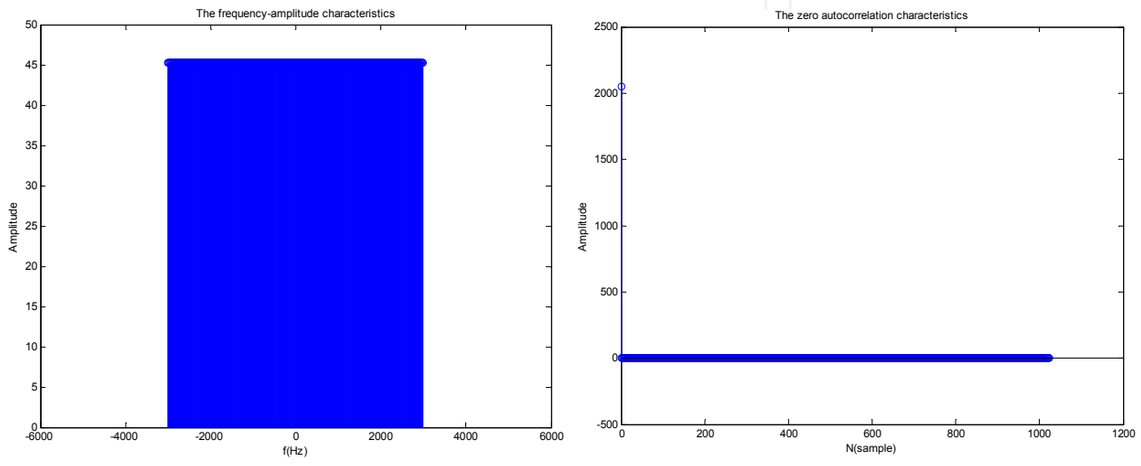

(a) (b)

Fig. 12. The CAZAC feature of the CHU sequence (a) constant amplitude (b) zero autocorrelation

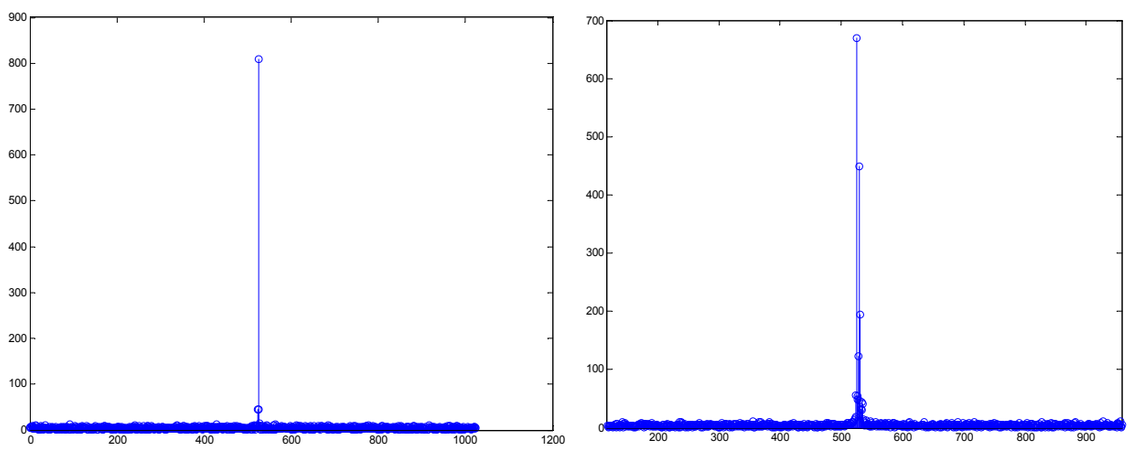

(a) (b)

Fig. 13. Channel impulse respond estimated by CI complex sequence (a) AWGN channel (b) 4-path Rayleigh channel

4.2.2 Frequency domain equalization

In the conceptual model of CI/OFDM, the information symbols are simultaneously modulated on multi-subcarrier which makes CI/OFDM inherently having the frequency diversity. At the receiver side, frequency combining may be used to improve the performance of the system.

We still focus on the multi-carrier algorithm which makes use of the properties of IDFT/DFT, such as the linearity and the circular shift. Since every parallel input signal of the second IDFT is the summation of information signals, which are spread by CI signal, the frequency diversity combining should be at the end of the first DFT module at the receiver side.At the receiver, after orthogonal multi-carrier demodulation, the output of the first FFT is

$$r_i = H_i \cdot \sum_{k=0}^{N-1} a_k e^{j\frac{2\pi}{N} \cdot i \cdot k} + n_i \tag{26}$$

where $i \in [1, N]$ is the number of the subcarrier, H_i is the transition function of the sub-channel and a_k is the information symbol, $k \in [1, N]$.

According to Fig. 15, the input signals at the second FFT module which can be expressed as

$$R_i = w_i r_i = w_i (H_i \sum_{k=0}^{N-1} a_k e^{j\frac{2\pi}{N} \cdot i \cdot k} + n_i) \tag{27}$$

where w_i is the gain of the ith subcarrier determined by different combining strategies. Since R_i includes all information about transmitted symbols, the second FFT not only is applied for decomposing the CI spreading into the subcarrier components, but also is used to complete the frequency combining.

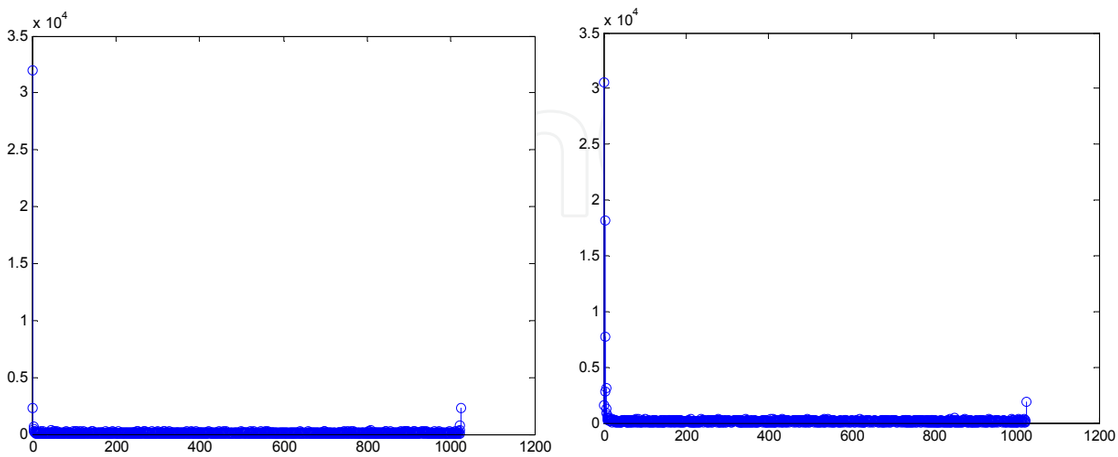

Fig. 14. Channel impulse respond estimated by CHU sequence (a) AWGN channel (b) 4-path Rayleigh channel

Several frequency combining strategies such as EGC, the MRC, orthogonal restoration combining (ORC) and MMSEC are considered in frequency selective channel (Itagkai & Adachi, 2004). Computer simulation results are shown in Fig. 16. In CI/OFDM system, though both combing strategies are sensitive to the inter-carrier interference (ICI), the MRC performance is worse than EGC. It is because that in MRC, the phase changes of the signals are lost, which is very important to CI/OFDM. Since ORC equalization perfectly restores frequency non-selective channel but produces the noise enhancement, its performance is better than MRC and EGC but worse than MMSEC. As SNR increases, the BER performance of ORC gets better, but MMSEC equalization provides the best performance. AS we know, the MMSEC not only restores frequency non-selective channel but also minimizes the noise.

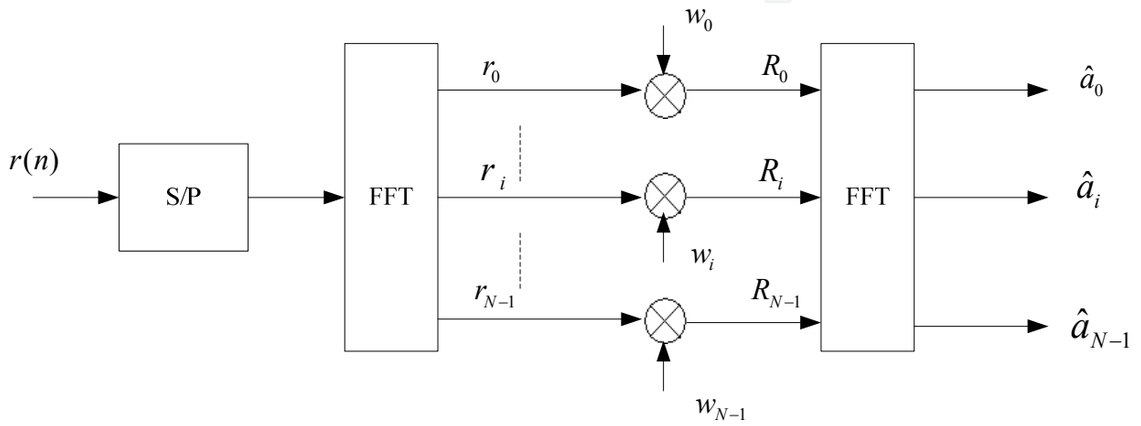

Fig. 15. Frequency combining in multi-carrier algorithm

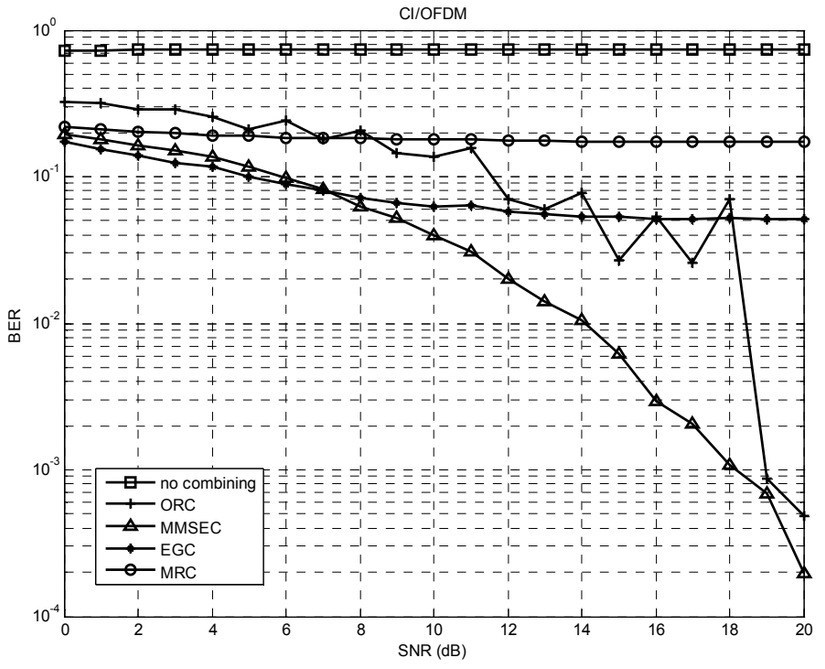

Fig. 16. Performance comparisons of ORC, MMSEC, EGC and MRC

5. Field test results

5.1 Experiment I

5.1.1 Experimental pool

The experimental pool in Xiamen University is an un-censored pool which size is 430(L)x320(W)x200(H)cm.

Channel estimation was carried out, 13kHz single carrier signal is sent at the 30ms intervals. The sample rate of A/D is 160kHz. The transmitted and received signals are shown in Fig. 17. We can see that key features of the channel are multi-path transmission with low noise because of the stationary water in the pool. The maximum delay is about 19 ms which magnitude is under 3% of the maximum one.

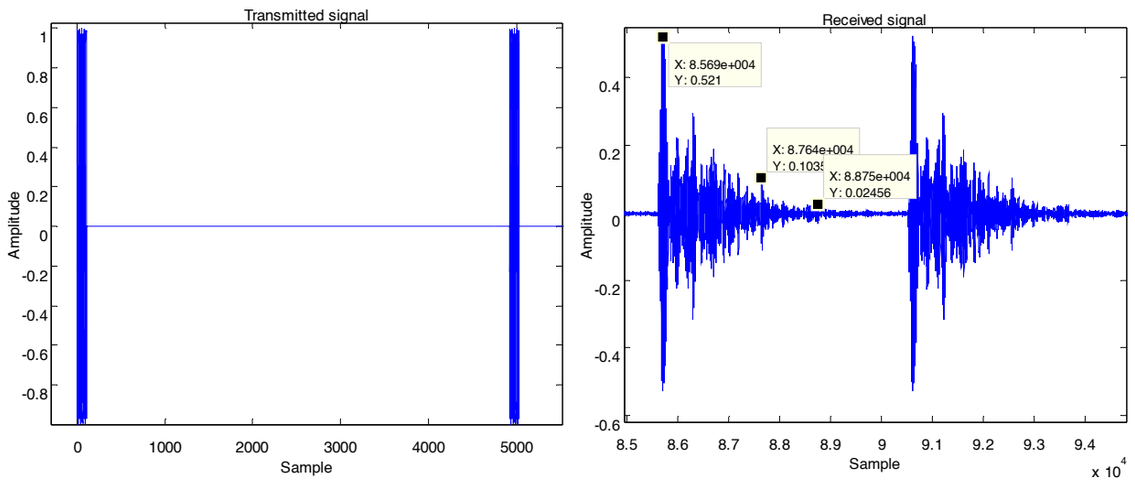

Fig. 17. The transmitted and received signal (13kHz)

5.1.2 Results of experimental pool

In this experiment, LFM signal was used to get coarse synchronization of the frame and CI complex sequence was applied to achieve accurate synchronization and fractional frequency shift estimation (Xu et al., 2008). SNR estimation algorithm is borrowed from the work (Ren, 2005) with synthesis of CI complex sequence. CI complex sequence is used as pilot to estimate the impulse response of the channel. Frequency-domain equalization ORC is used at the receiver to improve the performance of the system. Table 1 shows the parameters of the CI/OFDM system.

The results are shown in Table 2. Since the water in pool is stationary, the SNR is high and the average SNR is about 12dB. BER performance is good and the average fractional frequency shift is about 0.07Hz, which is very small compared with the subcarrier interval $\Delta f = 6000 / 1024 = 5.86 Hz$.

Baseband mapping	QPSK
Subcarrier mapping	Localized
Synchronization signal	LFM/CI complex spreading sequence
Pilot	CI complex sequence
Pilot pattern	Block
Equalization	ORC
Bandwidth	6kHz
Carrier frequency	13kHz
Sampling rate	156kHz
Number of the parallel signal	1024
System rate	4.97kbps

Table 1. System parameters

SNR (dB)	Fractional frequency shift (Hz)	BER
12.33659	0.068643	3.48771e-06

Table 2. BER performance

5.2 Experiment II

5.2.1 Shallow water in Wuyuan Bay of Xiamen

A CI/OFDM underwater acoustic communication experiment was conducted on Dec. 12, 2008 in Wuyuan Bay of Xiamen, China. The distance between the transmitter and the receiver was 1000m, and they were deployed at 3 m and 2 m below the sea-surface, respectively. The average depth of the water is 4. 5m which was changed with the tide. The channel probing signals include two kinds. One is a single carrier signal which was transmitted at the 100ms intervals repeatedly. The other is a sweeping signal which frequency is from 9kHz to 21kHz. It was also be transmitted once every 100ms.

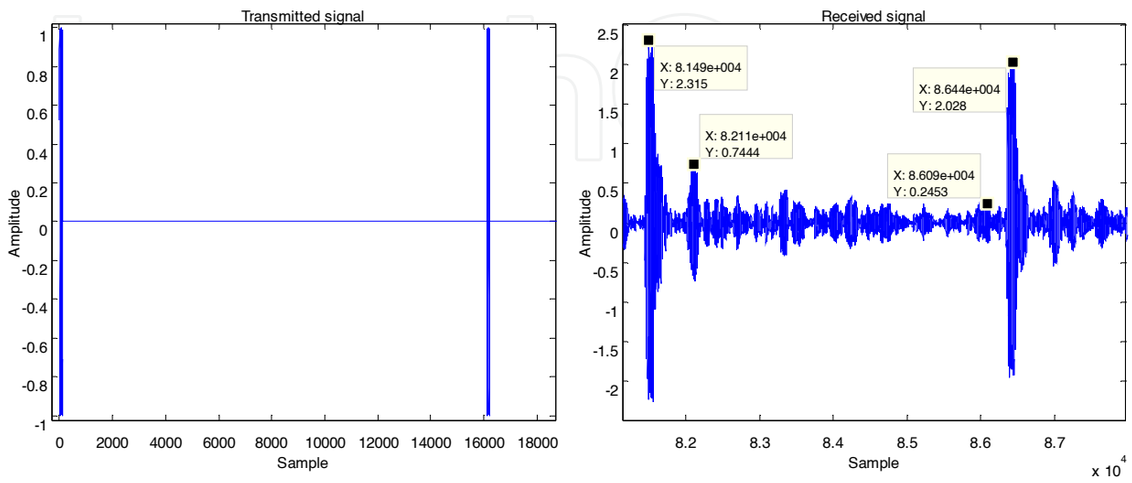

Fig. 18. Transmitted and received signal (14kHz)

As shown in Fig. 18, multi-path signals is visible during the 100ms intervals though the amplitude of the multi-path signal is about 2% of the maximum one. The amplitude of the 14KHz signal was changed after 100ms. Fig. 19 denotes the different amplitudes of the sweeping signals which reveal the time-varying and frequency-varying features of the acoustic underwater channel.

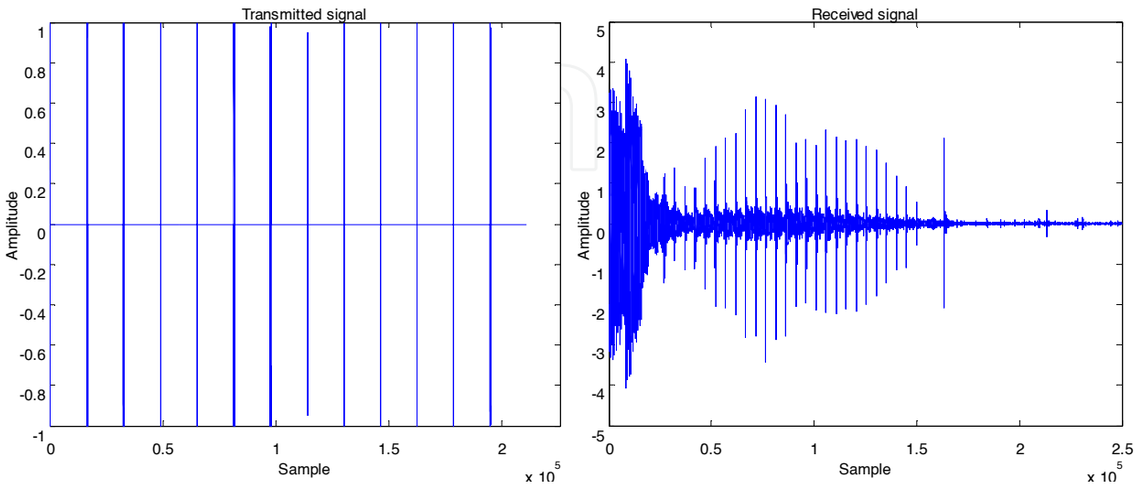

Fig. 19. Transmitted and received sweeping signal (9kHz to 21kHz)

5.2.2 Results of experiment II

Table 3 is the parameters of CI/OFDM underwater acoustic communication system. Table 4 is the BER performance of the system without and with frequency selective combining. The BER performance was significantly improved due to the frequency diversity combining by the cost of decrease of the data rate.

Baseband mapping	QPSK
Subcarrier mapping	Localized
Synchronization signal	LFM
Pilot	CI/OFDM signal
Pilot pattern	Block
Equalization	MMSEC
Bandwidth	5kHz
Carrier frequency	15kHz
Sampling rate	60kHz
Number of the parallel signal	1024
Data rate	4.97kbps/1.24kbps in 4-fold frequency diversity

Table 3. System parameters

BER (without frequency diversity)	BER (with 4-fold frequency diversity)
0.014257	0.0058714

Table 4. BER performance

5.3 Experiment III

5.3.1 Shallow water in Baicheng water

Two CI/OFDM underwater acoustic communication experiments were conducted on Dec. 17, 2009 and Dec. 31, 2009 in Baicheng water of Xiamen, China, respectively. The transmitter was deployed at 2.5m above the sea-floor in 5.5m deep water and the receiver was deployed at 9m below the sea-surface in 16m deep water. The horizontal distance between the transmitter and receiver were 2000m and 5000m, respectively.

The channel probing signals used in these two experiments were same sweeping signals, with frequency from 8KHz to 16KHz. The time interval between different frequencies was 30 ms.

Fig.20 is the received probing signal at the short range (2000m). The sea condition was calm but vessels passed through the water frequently. The Frequency-varying feature is different from the feature in Wuyuan Bay. In this experiment, the amplitudes of the lower and higher frequency were faded significantly. The ambient noise was much higher in this underwater channel. From the enlarged map of received signal of 14KHz and 14. 5KHz, it is easy to see that the amplitudes of the strongest arrival changed with time and frequencies. The high level of noise made it difficult to distinguish multi-path signals from the ambient noise. Note that there is no apparent impulse interference and the amplitudes of multi-path signals are much smaller than that of the main path.

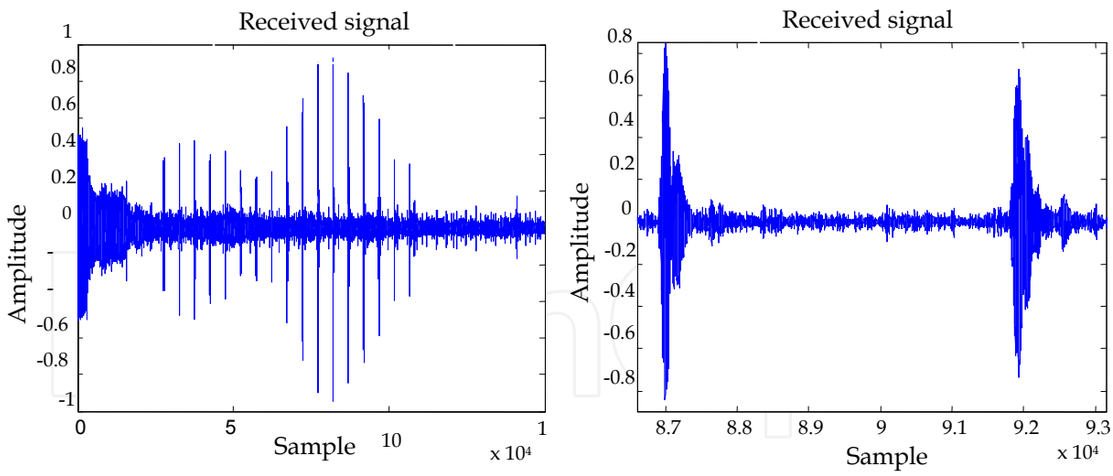

(a) (b)

Fig. 20. Received signals. (a) received sweeping signals (8kHz to 16kHz) (b) received single carrier signal (14kHz and 14.5kHz)

Fig. 21. is the transmitted and received probing signal at the long range (5000m). It was a windy day, and the sea condition was not calm. Many vessels passed through the water.

The Frequency-varying feature is different from the feature in short range at the same water domain. In this experiment, the ambient noise was much higher than that in the short range.

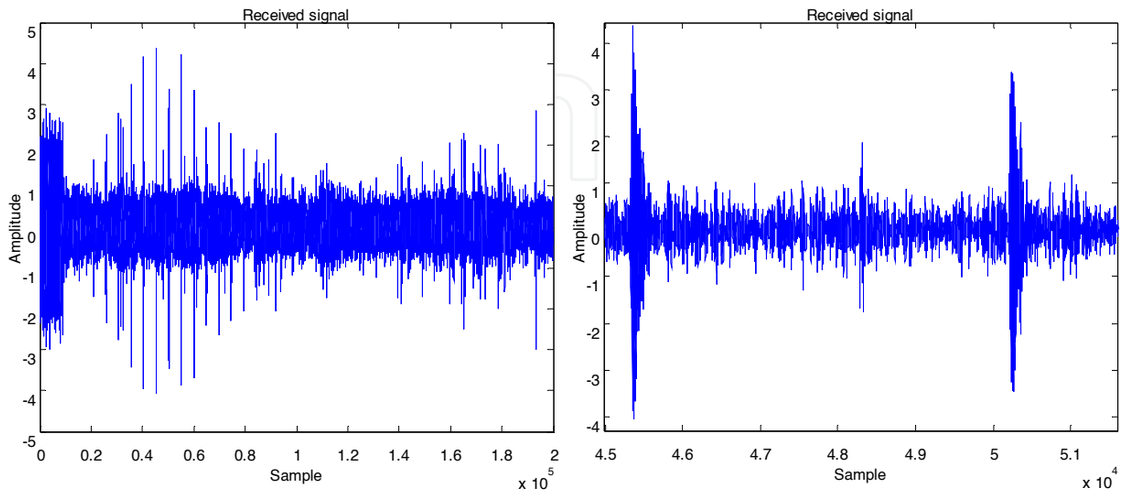

(a) (b)

Fig. 21. Received signals. (a) received sweeping signals (8kHz to 16kHz) (b) received single carrier signal (14kHz and 14.5kHz)

5.3.2 Results of experiment III

Based on the channel probing results, we concluded that the channel in Baicheng water was worse than that in Wuyuan Bay. In experiments, 4-fold frequency diversity and (2,1) LDPC were applied in CI/OFDM systems (Bai et al., 2009) in order to guarantee the BER performance of the system.

System parameters are same in Table 3 except that the comb pilot pattern is used instead of the block pilot. The results of using (2,1) LDPC is the performance improvement and the decrease of the data rate.

Date	BER (before LDPC decoding)	BER (after LDPC decoding)
Dec. 17, 2009	0.0393	0
Dec. 31, 2009	0.06598	0

Table 5. BER performance

Fig. 22 is the received CI/OFDM signals in short range (2000m) experiment. The amplitude of the received signal changed dramatically, and the level of ambient noise was high. There

was deeply frequency fading in the bandwidth of the signal. It might explain the reason of BER performance degradation even though the 4-fold frequency diversities were used.

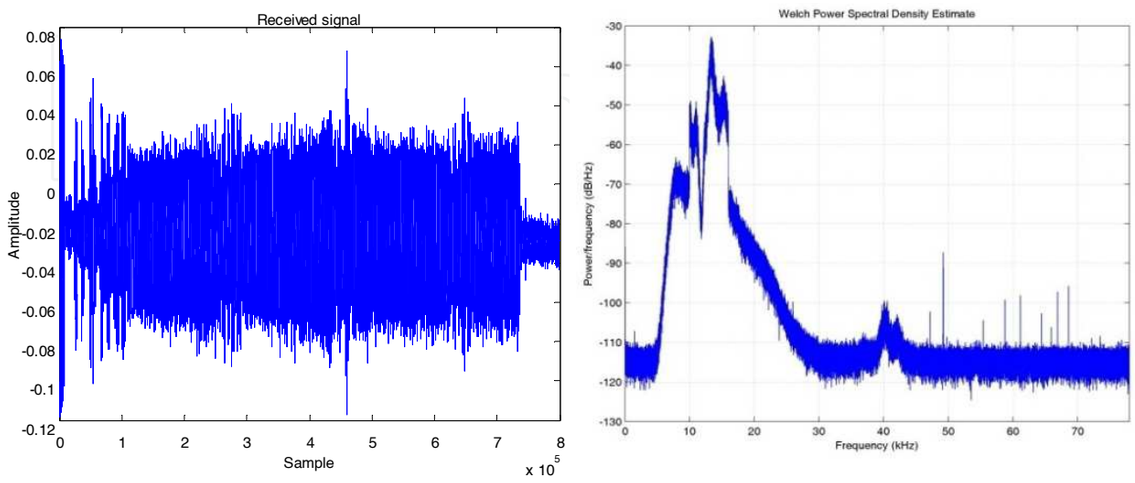

(a) (b)

Fig. 22. The received signal (a) the received profile (b) the power spectral density of the received signal

6. Conclusion

In this chapter, we first proposed two algorithms which simplify the modulation and demodulation of the conceptual CI/OFDM. Secondly, based on these algorithms and jointed with synchronization, channel estimation and equalization, we constructed CI/OFDM underwater acoustic communication systems. In the end, a number of experiments were carried out in the experimental pool and shallow waters in Xiamen of China to verify the performance of the system. Field results are as followed:

The BER of the uncoded CI/OFDM underwater acoustic communication system at the data rate 4.97kbps is lower than 4×10^{-6} in the experimental pool (experiment I) and 1.5×10^{-2} in Wuyuan Bay in Xiamen (experiment II). When 4-fold frequency diversity is applied, the data rate is 1.24kbps and the BER performance of the system is lower than 6×10^{-3} in experiment II.

The BER of the uncoded 4-fold frequency diversity CI/OFDM acoustic communication system at the data rate 1.24kbps is lower than 4×10^{-2} and 7×10^{-2} in experiment III at Baicheng water in Xiamen. The BER of the coded frequency diversity CI/OFDM acoustic communication system at the data rate 620bps is almost zero in the short range and the long range.

A few problems exist in the system. The most important one is that the inherent frequency diversity of CI/OFDM did not play its due role in the system. According to our analysis, the orthogonality between the different symbols modulated on the same subcarrier will be destroyed if the phases were changed when signals transmitted in the channel. It means that the intersymbol interference cancels out the diversity combining gain. Future researches should focus on the optimization of the algorithms in order to take advantage of the inherent frequency diversity and other realizations based on the conceptual CI/OFDM.

7. Acknowledgment

This work was supported by the Fundamental Research Funds for the Central Universities of China 2010121062.

8. References

Bai, L. Y., Xu, F., Xu, R & Zheng S. Y. (2009), LDPC Application Based on CI/OFDM Underwater Acoustic Communication System, *Proceedings of the First International Conference on Information Science and Engineering*, ISBN 978-0-7695-3887-7, Nanjing, Jiangsu China, December 26-December 28, 2009

Berkhovskikh, L. & Lysanov, Y. (2003). *Fundamentals of Ocean Acoustics (*3rd edition), Springer, ISBN 0-387-95467-8

CHU, D. C. (1972), Polyphase codes with good periodic correlation properties, *IEEE Transactions on information theory*, Vol. 18, Issue 4, pp. 531 - 532, July, 1972, ISSN 0018-9448

Freitag, L., Stojanovic, M, Singh, S. & Johnson M. (2001), Analysis of channel effects on direct-sequence and frequency-hopped spread-spectrum acoustic communication, *IEEE Journal of Oceanic Engineering*, Vol. 26, Issue 4, pp. 586-593, Oct 2001, ISSN 0364-9059

Frassati, F., Lafon, C., Laurent, P. A. & Passerieux, J. M. (2005), Experimental assessment of OFDM and DSSS modulations for use in littoral waters underwater acoustic communications, *Proceedings of Oceans 2005, Europe*, 20-23 June, 2005

Heimiller, R. C. (1961), Phase shift pulse codes with good periodic correlation properties, *IRE Transactions on Information Theory*, Vol. 7, Issue 4, pp. 254 - 257, October 1961, ISSN 0096-1000

Hlaing, M., Bhargava, V. K. & Letaief, K. B. (2003), A robust timing and frequency synchronization for OFDM systems, *IEEE Transactions on Communications*, Vol. 2, Issue 4, pp. 822 - 839, July 2003, ISSN 1536-1276

Itagkai, T. & Adachi F. (2004), Joint frequency domain equalization and antenna diversity combining for orthogonal multicode DS-CDMA signal transmissions in a frequency selective fading channel, *IEICE Transactions on Communications*, Vol. E87-B, No. 7, pp. 1954-1963, July 2004, ISSN 0916-8516

Jensen, F., Kuperman, W., Porter, M. & Schmidt H. (2011). *Computational Ocean Acoustics (*2nded), Springer,. ISBN 978-1441986771

Kim, B. C. & Lu, I. T. (2000), Parameter study of OFDM underwater communications system, *Proceedings of MTS/IEEE Conference and Exhibition OCEANS' 2000*, Providence, RI , USA, 11-14 Sept., 2000

Lam, W. K. and Ormondroyd R. F. (1997), A coherent COFDM modulation system for a time-varying frequency-selective underwater acoustic channel, P*roceedings of Seventh International Conference on Technology Transfer from Research to Industry, Electronic Engineering in Oceanography*, 23-25 June, 1997

Li, B. S., Zhou, S. L., Stojanovic, M., Freitag, L. & Willett, P. (2008), Multi-carrier communication over underwater acoustic channels with nonuniform Doppler shifts, *IEEE Journal of Oceanic Engineering*, Vol. 33, Issue 2, pp. 198-209, April 2008, I SSN: 0364-9059

Milewski, A. (1983), Periodic sequences with optimal properties for channel estimation and fast start-up equalization, *IBM Journal of Research and Development*, Vol. 27, Issue 5, pp. 426-431, Sept. 1983, ISSN 0018-8646

Nassar, C. R.; Natarajan, B. & Shattil, S. (1999). Introduction of carrier interference to spread spectrum multiple access, IEEE Emerging Technologies Symposium, Dallas, Texas,Apr 12-13, 1999

Nassar, C. R., Natarajan, B., Wu, Z., Wiegandt,D. A.; Zekavat S. A. & Shattil, S. (2002) *High-performance, Multi-carrier technologies for wireless communications*, Kluwer Academic Publishers, ISBN 0792-347618-8

Nassar, C. R., Natarajan, B., Wiegandt,D. A. & Wu, Z. (2002), Multi –carrier platform for wireless communications. Part 2: OFDM and MC-CDMA systems with high performance, high throughput via innovations in spreading, *Jornal of Wireless Communications and Mobile Computing*, Vol. 2, Issue 4, 2002. pp. 381-403, ISSN 1530-8677

Ren G. L., Chang Y. L., Zhang H, & Zhang H. N. (2005), Synchronization Method Based on a New Constant Envelop Preamble for OFDM Systems, *IEEE Transactions on Broadcasting*, Vol. 51, NO. 1, pp. 139-143, March 2005, ISSN 0018-9316

Rihaczek, A. W. (1977), *Principles of high-resolution radar*, Mark Resources, Inc. ISBN 978-0890069004

Shaw, A. and Srivastava, S. (2007), A Novel preamble structure for robust timing synchronization in OFDM system, *Proceedings of IEEE Region 10 Conference on TENCON,* ISBN 978-1-4244-1272-3, Taipei, China, Oct. 30 2007-Nov. 2 2007

Stojanovic, M. (1996), Recent advances in high-speed underwater acoustic communications, *IEEE Jounal of Oceanic Engineering*, Vo. 21, Issue 2, pp. 125–136, Apr. 1996. ISSN 0364-9059

Stojanovi, M., Proakis, J. G, Rice J. A. & Green, M.D.(1998), Spread spectrum underwater acoustic telemetry, Proceedings of Oceans 98, Nice, France Sep28 - Oct 1, 1998

Stojanovic & M. Freitag, L (2006), Multichannel Detection for Wideband Underwater Acoustic CDMA Communications, *IEEE Journal of Oceanic Engineering*, Vol. 31, Issue 3, pp. 685-695, July 2006, ISSN 0364-9059

Stojanovic, M. (2006), Low complexity OFDM detector for underwater acoustic channels, *Proceedings of MTS/IEEE Conference and Exhibition OCEANS' 2006,* Boston, Massachusetts, USA, 18-21 Sept. 2006

Stojanovic, M. (2007). On the Relationship Between Capacity and Distance in an Underwater Acoustic Channel, *ACM SIGMOBILE - Mobile Computing and Communications Review,* vol. 11, No. 4, Oct. 2007, pp. 34–43, ISSN: 1559-1662

Stojanovic, M. (2008), OFDM for underwater acoustic communications: adaptive synchronization and sparse channel estimation, *Proceedings of IEEE International Conference on Acoustics, Speech and Signal Processing*, ISSN 1520-6149, Las Vegas, NV, March 31 2008-April 4, 2008

Stojanovic, M. & Preisig, J. (2009). Underwater Acoustic Communication Channels: Propagation Models and Statistical Characterization, *IEEE Communications Magazine,* Vol. 47, Issue 1, Jan. 2009, pp. 84-89, ISSN 0631-6804

Tsimenidis, C. C., Hinton, O. R., Adams, A. E. & Sharif, B. S. (2001), Underwater acoustic receiver employing direct-sequence spread spectrum and spatial diversity combining for shallow-water multiaccess networking, *IEEE Journal of Oceanic Engineering*, Vol. 26, Issue 4, pp. 594-603, Oct 2001, ISSN 0364-9059

Wiegandt,D. A. & Nassar, C. R. (2001). High Performance OFDM via carrier interferometry, *Proceedings of IEEE International Conference on Third Generation Wireless and Beyond (3Gwireless '01)*, San Francisco, CA, May 30, 2001

Wiegandt,D. A.&Nassar, C. R. (2001), "Crest Factor Considerations in MC-CDMA with Carrier Interferometry Codes," *Proceedings of IEEE Pacific-Rim Conference on Communications,Computers and Signal Processing*, Victoria, Canada, August 26-28, 2001

Wiegandt,D. A.; Nassar, C. R. &Wu Z. (2001). Overcoming peak-to-average power ratio issues in OFDM via carrier interferometry codes, *Proceedings of IEEE International Conference on Vehicular Technology*, Atlantic City, NJ, USA, Oct. 7-11, 2001.

Wiegandt,D. A.&Nassar, C. R. (2003). High-throughput, high-performance OFDM via pseudo-orthogonal carrier interferometry spreading codes. *IEEE transaction of Communications*, Vol. 51, Issue 7, July 2003, pp. 1123-1134, ISSN 0090-6778

Wiegandt,D. A.; Nassar, C. R. &Wu Z. (2004). The elimination of peak-to-average power ratio concerns in OFDM via carrier interferometry spreading codes: a multiple constellation analysis, *Proceedings of the Thirty-Sixth Southeastern Symposium on System Theory*, March 14-16, 2004

Xu, F., Hu, X.Y. & Xu, R. (2007), A Novel Implementation of Carrier Interferometry OFDM in an Underwater Acoustic Channel, *Proceedings of Oceans 2007,* ISBN 978-1-4244-0635-7, Aberdeen, *UK,* 18-21 June 2007

Xu, F., Xu, R. & Sun H. X. (2007), Implementation of Carrier Interferometry OFDM by Using Pulse Shaping Technique in Frequency Domain, *Proceedings of IEEE International Workshop on Anti-counterfeiting, Security, Identification*, ISBN 1-4244-1035-5, Xiamen, Fujian, China, 16-18 April, 2007

Xu, F. Xu, R., Zhang Y. H., Sun H. X. & Wang, D. Q. (2008), Design and test of a carrier interferometry OFDM system in underwater acoustic channels, *Proceedings of IEEE International Conference on Communications, Circuits and Systems,* ISBN 978-1-4244-2063-6, Fujian, China, 25-27 May, 2008

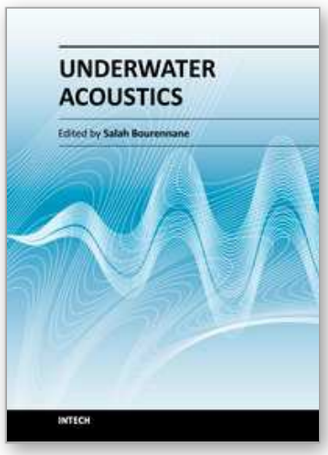

Underwater Acoustics

Edited by Prof. Salah Bourennane

ISBN 978-953-51-0441-4
Hard cover, 136 pages
Publisher InTech
Published online 28, March, 2012
Published in print edition March, 2012

How to reference

In order to correctly reference this scholarly work, feel free to copy and paste the following:

Fang Xu and Ru Xu (2012). CI/OFDM Underwater Acoustic Communication System, Underwater Acoustics, Prof. Salah Bourennane (Ed.), ISBN: 978-953-51-0441-4, InTech, Available from: http://www.intechopen.com/books/underwater-acoustics/ci-ofdm-underwater-acoustic-communication-system

INTECH
open science | open minds

InTech Europe
University Campus STeP Ri
Slavka Krautzeka 83/A
51000 Rijeka, Croatia
Phone: +385 (51) 770 447
Fax: +385 (51) 686 166
www.intechopen.com

InTech China
Unit 405, Office Block, Hotel Equatorial Shanghai
No.65, Yan An Road (West), Shanghai, 200040, China
中国上海市延安西路65号上海国际贵都大饭店办公楼405单元
Phone: +86-21-62489820
Fax: +86-21-62489821

IntechOpen